Electric transport and magnetic properties of perovskites $LaMn_{1-x}Co_xO_3$ up to 900 K

2005 J. Phys.: Condens. Matter 17 1601

(http://iopscience.iop.org/0953-8984/17/10/015)

INSTITUTE OF PHYSICS PUBLISHING JOURNAL OF PHYSICS: CONDENSED MATTER

J. Phys.: Condens. Matter **17** (2005) 1601–1616 doi:10.1088/0953-8984/17/10/015

Electric transport and magnetic properties of perovskites $LaMn_{1-x}Co_xO_3$ up to 900 K

C Autret[1,3], J Hejtmánek[1,4], K Knížek[1], M Maryško[1], Z Jirák[1], M Dlouhá[2] and S Vratislav[2]

[1] Institute of Physics, Cukrovarnická 10, 162 53 Prague 6, Czech Republic
[2] Faculty of Nuclear Physics and Physical Engineering, Brehová 7, 115 19 Prague 1, Czech Republic

E-mail: hejtman@fzu.cz

Received 3 December 2004, in final form 7 February 2005
Published 25 February 2005
Online at stacks.iop.org/JPhysCM/17/1601

Abstract

The structural, magnetic and transport properties of the $LaMn_{1-x}Co_xO_3$ system were investigated over a wide temperature range, 10–900 K. Two structural types, depending on x, were detected—orthorhombic $Pbnm$ ($x \leqslant 0.5$) and rhombohedral $R\bar{3}c$ ($x > 0.6$), separated by the bi-phasic sample $x = 0.6$. At both ends of the $LaMn_{1-x}Co_xO_3$ system, the respective substituents are unambiguously characterized as Co^{2+} ($x \leqslant 0.1$) and Mn^{4+} ($x \geqslant 0.9$). On the Mn-rich side, up to $x < 0.5$, we infer on the basis of high temperature transport and magnetic data the gradual increase of the Co^{2+} valence towards the prevailing Co^{3+}, while for the Co-rich samples ($0.6 \leqslant x \leqslant 0.8$), the Co^{3+} states tend to disproportionate at high temperatures to $Co^{2+} + Co^{4+}$, which probably controls both the transport and magnetic properties. At low temperatures, the long range ferromagnetic order was confirmed by means of neutron diffraction for the $x = 0.4$ sample. A non-uniform magnetic state was detected at higher cobalt substitution up to $x = 0.8$ and was associated with FM clusters that are formed below ∼220 K and coagulate below ∼150 K.

(Some figures in this article are in colour only in the electronic version)

1. Introduction

Recently a lot of studies were performed on perovskite manganites and cobaltites, because of their interesting magnetic and transport properties resulting from the competition of the lattice, charge, spin and orbital degrees of freedom [1, 2]. The perovskites are structurally very simple systems of formula AMO_3, where A is either a rare earth (La, Pr . . .) or an alkaline earth such

[3] Present address: Laboratoire LEMA, Faculté des Sciences et Techniques, Parc Grandmont, 37200 Tours, France.
[4] Author to whom any correspondence should be addressed.

as Ca, Sr, Ba and M is a 3d transition metal (Mn, Co). The prototype perovskite manganite is the $LaMnO_3$ compound that exhibits an orthorhombic structure with the *Pbnm* space group symmetry (see e.g. [3]). The compound is insulating and becomes antiferromagnetic (AFM) below the Néel temperature ($T_N \approx 140$ K). The Mn valency is 3+ in the high spin (HS) state ($3d^4$ configuration, $S = 2$). The AFM state is of the A type, which is described in terms of ferromagnetic (FM) planes that are coupled antiferromagnetically. However, when $LaMnO_3$ is synthesized in air, an excess of oxygen in the perovskite lattice is observed. This corresponds in fact to La and Mn vacancies, and both the magnetic and transport properties depend critically on this oxygen excess in $LaMnO_{3+\delta}$ [4, 5]. The analogous $LaCoO_3$ compound crystallizes in rhombohedral symmetry and is a diamagnetic insulator at low temperatures with a low spin (LS) state of Co^{3+} ($3d^6$, $S = 0$). This compound undergoes a gradual transition from the LS to the paramagnetic state, centred at about 100 K. The uniform state, achieved at 200–300 K, was initially explained as the ordered mixture of the LS and the high spin (HS, $S = 2$) states [6], but in the recent literature, stabilization of the intermediate spin (IS, $S = 1$) state is frequently claimed [7–12].

Considerable attention was attracted to solid solutions $LaMn_{1-x}Co_xO_3$ with dominant FM interactions, too. Goodenough *et al* concluded in their early work that the superexchange interactions between Mn^{3+} neighbours are probably responsible for the FM state in the samples with $0 < x \leqslant 0.5$ provided that static Jahn–Teller distortions are absent [13]. Later on, the main FM interactions in the $LaMn_{0.5}Co_{0.5}O_3$ compound were associated with the positive superexchange between stabilized Co^{2+} and Mn^{4+} pairs [14]. On the other hand, Park *et al* argued that the FM coupling should be associated with the double exchange due to the Mn^{3+}/Mn^{4+} coexistence [15]. Troyanchuk discussed the magnetic properties of $LaMn_{1-x}Co_xO_3$ in terms of the competition between positive Mn^{3+}–O–Mn^{4+}, Mn^{3+}–O–Mn^{3+}, Co^{2+}–O–Mn^{4+} and negative Mn^{4+}–O–Mn^{4+}, Co^{2+}–O–Co^{2+}, Mn^{3+}–O–Co^{2+} superexchange interactions, considering also a tendency to Co^{2+} and Mn^{4+} ionic ordering of NaCl type [16]. A similar hypothesis was applied in the recent paper of Dass and Goodenough [17]. Most recent studies report the existence of two FM phases for $x \sim 0.5$, i.e. for $LaMn_{0.5}Co_{0.5}O_3$, depending on the preparation conditions [16–19]. Joy *et al* demonstrated that the phase with higher $T_C = 225$ K forms in the low temperature synthesis at about 700 °C while the phase with lower $T_C = 150$ K can be prepared in the high temperature method by quenching from 1300 °C [18, 19]. Other routes to obtaining a single FM phase of $LaMn_{0.5}Co_{0.5}O_3$ were described recently, as well [16, 17]. It appears that the higher $T_C = 225$ K is associated with the Co^{2+}/Mn^{4+} (1:1) order and the ordered phase also exhibits the highest spontaneous moment close to the theoretical 3 μ_B for HS Co^{2+} and Mn^{4+} ions. The neutron diffraction data suggest that the degree of ordering can be as high as 90% [20], but commonly prepared samples show generally only short range order with a significant amount of disordered phase probably associated with local fluctuations in the cationic composition, oxygen deficiency etc.

In this paper we report on the structural, magnetic and transport properties of the $LaMn_{1-x}Co_xO_3$ system over a wide temperature range, 10–900 K. Our attention is focused on the non-uniform states in compositions close to $x \approx 0.5$ and phase transitions at the Co-rich end of the series. On the basis of the magnetic susceptibility and the thermoelectric power data, we discuss possible valence and spin states of the Mn and Co cations, respectively.

2. Experiments

The $LaMn_{1-x}Co_xO_3$ compounds were prepared by solid state reaction at high temperatures. Homogenized mixtures of the respective oxides and carbonates were calcined at 900 °C to achieve decarbonation. The pre-reacted powder was pressed into the form of pellets that

were briefly heated in air to 1500 °C (1 h duration) before undergoing a prolonged sintering at 1300 °C (40 h). The pellets were then cooled to the room temperature by switching off the furnace. Since the Mn-rich compounds ($x \leqslant 0.4$) showed a cationic deficiency after the sintering in air, they were subsequently annealed at 1100 °C under a vacuum of 10^{-3} mbar for two days.

The powder x-ray patterns were recorded by using a Bruker D8 diffractometer with Cu Kα radiation, the powder neutron diffraction study was carried out using a KSN-2 diffractometer in Rez near Prague, using a wavelength $\lambda = 1.360$ Å. The diffraction patterns were analysed with the Rietveld method using the FULLPROF program.

Measurements of the electrical resistivity and thermoelectric power were carried out using the four-point method, i.e. with separated power and effect (voltage, temperature) contacts. The low temperature set-up (12–310 K) employed a closed-cycle He refrigerator and the thermal gradient was generated by a miniheater and measured using the E-type thermocouples. For the high temperature measurements (300–900 K) the sample was placed on a ceramic sample holder centred in the small tubular furnace with a precisely controlled temperature. Standard K-type thermocouples were used for temperature monitoring; a controlled gradient of about 5 K was imposed across the sample by means of an additional furnace.

The magnetic susceptibility was measured using a SQUID magnetometer in the range up to 400 K under a DC field of 100 Oe while the high temperature data up to 800 K were obtained using a compensated pendulum system, MANICS, in a field of 3000 Oe.

3. Results

Powder XRD patterns registered at room temperature confirmed a perovskite phase formation for all the solid solutions $LaMn_{1-x}Co_xO_3$ ($0 \leqslant x \leqslant 1$). The refined structural parameters are summarized in table 1 ($0 \leqslant x \leqslant 0.6$) and in table 2 ($0.6 \leqslant x \leqslant 1$). The results show two structural types depending on the x. For $x = 0$–0.5, the diffraction patterns are indexed in an orthorhombic perovskite structure of the $GdFeO_3$ type (space group $Pbnm$) with unit cell parameters close to $a_p\sqrt{2}$, $a_p\sqrt{2}$, $2a_p$ where $a_p \approx 3.9$ Å is related to the cubic perovskite. On the other hand, the reflections for the samples $0.6 < x \leqslant 1$ are indexed in a rhombohedral structure with the $R\bar{3}c$ space group, similarly to the pure $LaCoO_3$ compound. The unit cell parameters are close to $a_p\sqrt{2}$, $\gamma = 60°$ or, in the more common hexagonal setting, $a_h = a_p\sqrt{2}$, $c_h = 2a_p\sqrt{3}$, $\gamma = 120°$. The sample with $x = 0.6$ exhibits both kinds of perovskite structure and the refinement leads to ratios of ~60% for the orthorhombic phase and of ~40% for the rhombohedral phase. We have tried to anneal this sample under different atmospheres, but the bi-phasic character did not change, in agreement with the previous observation of Voronin *et al* [21].

An important additional question is that of the oxygen stoichiometry of the present samples. As regards pure $LaMnO_3$, we may refer to neutron powder diffraction data given by Rodriguez-Carvajal *et al* [3], included also in table 1. The comparison of the data in the first two columns reveals that the unit cell volume of our compound is slightly smaller. This means that our sample, despite the additional annealing under vacuum, is slightly off-stoichiometric with a formal excess in oxygen. Using the notation $LaMnO_{3+\delta}$, the actual δ value is approximately equal to 0.02 (see e.g. [4]). On the other hand, the similarly treated Co-substituted samples with $x = 0.1$–0.3 and air-prepared samples with $x \geqslant 0.4$, which do not exhibit any volume change after the vacuum annealing, are probably stoichiometric. In particular, $LaCoO_3$ in table 2 shows the same unit cell volume as was reported for this compound by Vogt *et al* [22].

Figures 1 and 2 present the evolution of the lattice parameters and unit cell volume, over the whole range of solid solutions. A large O′ type of orthorhombic deformation in $LaMnO_3$,

Table 1. Crystallographic parameters from x-ray diffraction studies at room temperature for the $LaMn_{1-x}Co_xO_3$ system ($0 \leqslant x \leqslant 0.6$). The $x = 0$ results are from [3].

x	0 (NPD) Ref. [3]	0	0.1	0.2	0.4	0.5	0.6a 59(1)%
S.G.	*Pbnm*	*Pbnm*	*Pbnm*	*Pbnm*	*Pbnm*	*Pbnm*	*Pbnm*
a (Å)	5.5367(1)	5.5347(2)	5.5317(2)	5.5355(2)	5.5273(2)	5.5191(5)	5.5105(5)
b (Å)	5.7473(1)	5.7043(2)	5.5837(3)	5.5261(3)	5.4949(2)	5.4768(5)	5.4654(5)
c (Å)	7.6929(2)	7.7029(2)	7.7910(3)	7.8133(4)	7.7807(2)	7.7635(2)	7.7409(6)
V (Å^3)	244.79	243.2	240.65	239.01	236.32	234.67	233.13
La							
x	−0.0078(3)	−0.0074(4)	−0.0061(6)	−0.0063	−0.0063(3)	−0.005(1)	−0.005
y	0.0490(3)	0.0449(3)	0.0339(3)	0.0297(4)	0.0237(2)	0.0212(3)	0.0212
z	0.25	0.25	0.25	0.25	0.25	0.25	0.25
Co, Mn							
x	0.5	0.5	0.5	0.5	0.5	0.5	0.5
y	0	0	0	0	0	0	0
z	0	0	0	0	0	0	0
O_{ap}							
x	0.0745(3)	0.079(3)	0.076(5)	0.053	0.056(4)	0.050(8)	0.050
y	0.4874(3)	0.488(3)	0.489(4)	0.485(4)	0.494(2)	0.501(3)	0.501
z	0.25	0.25	0.25	0.25	0.25	0.25	0.25
O_{eq}							
x	0.7256(2)	0.725(3)	0.726(4)	0.718(6)	0.728(3)	0.735(7)	0.735
y	0.3066(2)	0.302(2)	0.287(3)	0.278(6)	0.281(3)	0.261(7)	0.261
z	0.0384(2)	0.038(2)	0.032(2)	0.033	0.033(2)	0.035(3)	0.035
R_{Bragg} (%)	5.16	6.58	7.03	12.6	3.72	8.43	3.02
χ^2	2.35	2.05	1.44	1.81	1.32	1.41	1.47
Mn–O_{ap} (Å) (×2)	1.9680(3)	1.976(4)	1.994(6)	1.972(1)	1.970(3)	1.961(6)	1.966(2)
Mn–$O1_{eq}$ (Å) (×2)	1.907(1)	1.92(1)	1.94(2)	1.98(3)	1.98(1)	1.95(3)	1.92(1)
Mn–$O2_{eq}$ (Å) (×2)	2.178(1)	2.14(1)	2.04(2)	1.99(3)	1.98(1)	1.98(3)	1.96(1)
Mn–O_{ap}–Mn (°)	155.48(2)	153.9(1)	155.2(2)	162.1(2)	161.0(1)	163.7(2)	153.6(2)
Mn-O_{eq}–Mn (°)	155.11(5)	155.9(6)	160.0(9)	159(1)	157.3(6)	163(1)	163.4(1)

characterized by the ratio $b > a > c/\sqrt{2}$, is a direct consequence of the e_g orbital order (cooperative Jahn–Teller (JT) effect) associated with the Mn^{3+} cations. The MnO_6 octahedra are characterized by one long and one short Mn–O distance in the equatorial plane. With the Co substitution, the difference between the two Mn(Co)–O equatorial distances decreases quickly and the lattice system becomes pseudocubic at $x = 0.2$. For higher x another kind of the deformation develops, characterized by the reversed ratio $a > c/\sqrt{2} \cong b$ of the lattice parameters. In the inset of figure 1 we compare the system $LaMn_{1-x}Ga_xO_3$ where a decrease of JT distortion with x is also observed [23]. Nonetheless, in agreement with the facts that the Ga^{3+} ions are inactive in the formation of covalent bonds with oxygen and do not affect the manganese valence state, the removal of JT distortion is not so 'rapid' as in the case of cobalt substitution. This different behaviour suggests that, at least in the orthorhombic $LaMn_{1-x}Co_xO_3$ compounds, the charge equilibrium is shifted from the $Mn^{3+} + Co^{3+}$ towards $Mn^{4+} + Co^{2+}$ coexistence. After the phase boundary at $x = 0.6$ is reached, the Co-rich samples with the rhombohedral structure show, with increasing x, linearly decreasing a and α parameters.

The unit cell volumes in $LaMn_{1-x}Co_xO_3$, displayed in figure 2, decrease smoothly with increasing Co content in both the orthorhombic and rhombohedral domains. This experimental

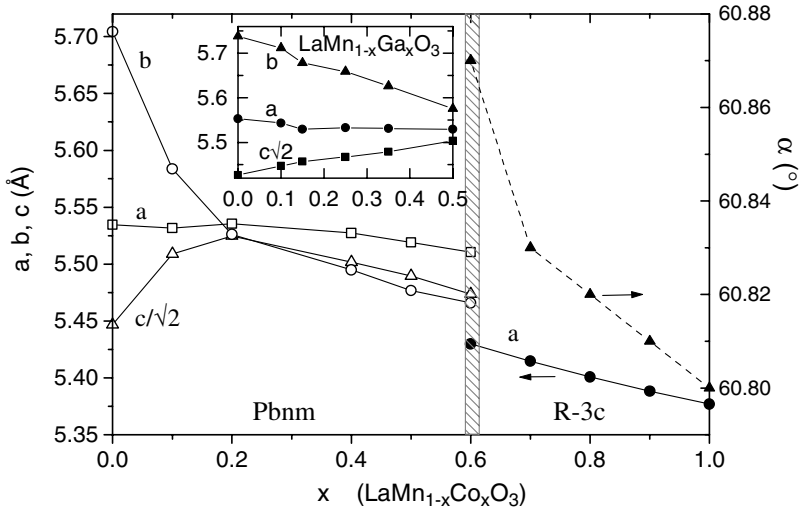

Figure 1. The composition dependence of the lattice parameters for $LaMn_{1-x}Co_xO_3$ solid solution. The *Pbnm* structures ($x = 0$–0.5) and $R\bar{3}c$ structures ($x = 0.7$–1) are separated by a bi-phasic compound $x = 0.6$. The inset shows the lattice parameters of $LaMn_{1-x}Ga_xO_3$ for comparison.

Table 2. Crystallographic parameters from x-ray diffraction studies at room temperature for the $LaMn_{1-x}Co_xO_3$ system ($0.6 \leqslant x \leqslant 1$). The $x = 1$ results are from [22].

x	0.6*b* 41(1)%	0.7	0.8	0.9	0.95	1	1 (ESR) Ref. [22]
S.G.	$R\bar{3}c$	$R\bar{3}c$	$R\bar{3}c$	$R\bar{3}c$	$R\bar{3}c$	$R\bar{3}c$	$R\bar{3}c$
a (Å)	5.5018(3)	5.4827(3)	5.4679(3)	5.4544(1)	5.4488(1)	5.4427(1)	5.442 63(3)
c (Å)	13.2111(7)	13.1791(9)	13.1468(8)	13.1170(3)	13.1045(3)	13.0899(3)	13.091 08(8)
V (Å^3)	346.33	343.09	340.41	337.95	336.95	335.81	335.834
La							
x	0	0	0	0	0	0	0
y	0	0	0	0	0	0	0
z	0.25	0.25	0.25	0.25	0.25	0.25	0.25
Co, Mn							
x	0	0	0	0	0	0	0
y	0	0	0	0	0	0	0
z	0	0	0	0	0	0	0
O							
x	0.445	0.445(2)	0.448(1)	0.453(1)	0.444(1)	0.437(1)	0.4488(7)
y	0	0	0	0	0	0	0
z	0.75	0.75	0.75	0.75	0.75	0.75	0.75
R_{Bragg} (%)	2.77	7.2	3.61	4.83	6.9	9.4	—
χ^2	1.47	1.45	2.66	1.47	2.18	3.06	2.765
Mn/Co–O (Å) (×6)	1.955(1)	1.949(2)	1.942(1)	1.933(1)	1.938(1)	1.939(2)	1.9329(5)
Mn/Co–O–Mn/Co (°)	162.39(1)	162.40(6)	163.23(4)	164.97(5)	162.05(5)	160.82(7)	163.4

observation is very important as, consistently with Vegard's law, a linear variation of the volume as a function of x is associated with a random distribution of the Mn and Co ions in the lattice, excluding thus the possibility of long range Mn/Co order.

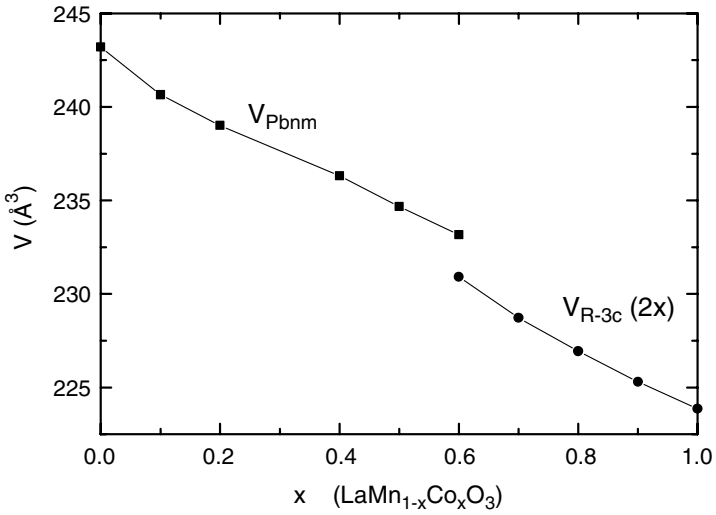

Figure 2. The composition dependence of the unit cell volume for $LaMn_{1-x}Co_xO_3$ solid solutions for the *Pbnm* structures ($Z = 4$) and $R\bar{3}c$ structures ($Z = 2$). The volume of the $R\bar{3}c$ structures is multiplied by 2 for comparison.

An overview of magnetic properties of the whole $LaMn_{1-x}Co_xO_3$ system was reported previously by Troyanchuk *et al* [16]. The A-type AFM order of pure $LaMnO_3$ was found to transform gradually to a FM state for $x \approx 0.15$; then the spontaneous moment decreased slowly with further Co substitution while the Curie temperature increased and reached a maximum for samples close to $x = 0.5$.

Consequently, the present work is mainly focused on $LaMn_{0.6}Co_{0.4}O_3$ ($x = 0.4$) which is displaced chemically from the commensurate Mn:Co (1:1) ratio and structurally from the crystallographic boundary at $x = 0.6$, but still keeps bulk FM order. The temperature dependence of the magnetization of $LaMn_{0.6}Co_{0.4}O_3$ in an applied field of $H = 5000$ Oe after zero-field cooling is shown in figure 3. The two-step transition, as frequently reported in the literature for $x = 0.5$, is also evident and becomes even more pronounced if the DC susceptibility is measured in a field of 100 Oe (see the upper panel of figure 4). Here, the magnetic susceptibility $\chi(T)$ curve shows a very sharp peak at 220 K, then a minimum is observed and a second much broader peak appears at about 150 K.

The structure and magnetic state of $LaMn_{0.6}Co_{0.4}O_3$ were investigated in more detail using neutron powder diffraction at three temperatures, −300, 160 and 10 K. These experiments confirmed unambiguously the existence of a long range ferromagnetic order (coherence length $\xi > 1000$ Å) even in the intermediate range 150–200 K, while no extra peaks that could be attributed to an eventual AFM phase were observed down to the lowest temperatures. The ordered FM moments were determined by the Rietveld analysis of diffraction patterns to be 1.15(9) μ_B at 160 K and 2.31(6) μ_B at 10 K, respectively. These values are in good agreement with magnetization extrapolated from the $M(H)$ curves shown in figure 5. Apart from a common lattice contraction, only little change was observed between the room and low temperature structural data when using a trial refinement; the possibility of long range Mn/Co order was unambiguously excluded. The detailed analysis of the lattice parameters and atomic coordinates obtained in the structural refinement using the neutron diffraction data of $LaMn_{0.6}Co_{0.4}O_3$ goes, however, beyond the scope of this paper and will be published elsewhere. It is of interest that similar, though pronounced, two-peak character of the susceptibility is

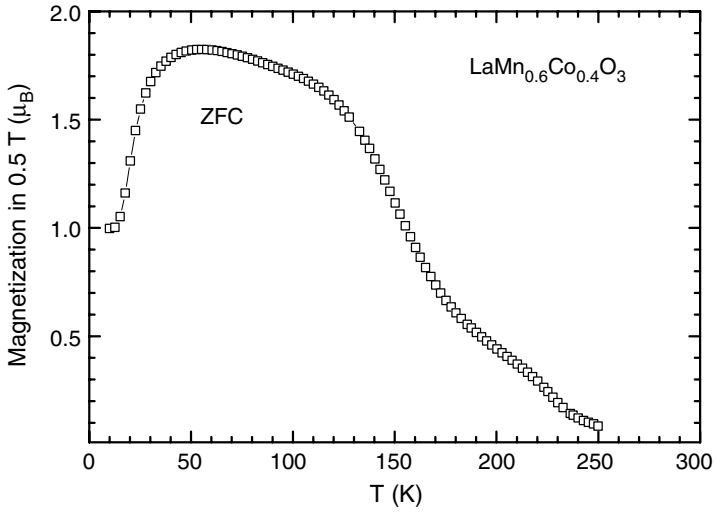

Figure 3. The temperature evolution of the magnetic moment of $LaMn_{0.6}Co_{0.4}O_3$ under a field of 0.5 T.

observed also for rhombohedral samples, in particular for $x = 0.8$ ones (see the lower panel of figure 4). In agreement with the previous report of Troyanchuk [16], an extremely large difference between FC and ZFC magnetization is observed. The bifurcation of the curves starts below $T \approx 220$ K, the same critical temperature as for the $x = 0.4$ sample, and develops with lowering of the temperatures, showing a notable anomaly at the second characteristic temperature $T \approx 150$ K. These observations suggest a highly non-uniform magnetic state in $LaMn_{0.2}Co_{0.8}O_3$ too, consisting below 220 K of fluctuating short range ordered FM regions embedded in the disordered matrix and their coagulation and freezing at 150 K. Comparison of peak heights at $T \approx 150$ K in ZFC curves for $x = 0.4$ and 0.8 samples allows us to estimate that the FM regions in the sample $LaMn_{0.2}Co_{0.8}O_3$ form a minor fraction only. Consequently, the marked peak observed on the ZFC curve at 25 K might be attributed to a spin glass transition which occurs in the dominating magnetically disordered regions.

The magnetic and valence states of the $LaMn_{1-x}Co_xO_3$ solid solutions in a broader compositional range, $0.4 \leqslant x \leqslant 1$, are illustrated using the plot of inverse susceptibility in figure 6. Strong FM interactions in the paramagnetic region are evidenced for the $x = 0.4$ and 0.5 samples, followed by the two-step transition at 220 and 150 K. In fact, the inverse susceptibility for these samples changes its slope slightly on heating above the room temperature and the effective moments actually obtained are $\mu_{\text{eff}} \sim 4.2\ \mu_B$ above 500 K (the corresponding spin value $S \sim 1.7$) and $\mu_{\text{eff}} \sim 4.7$ ($S \sim 1.9$) below 500 K. We note that these values are significantly larger than moments derived previously by Joy *et al* [18]. The linear Curie–Weiss form of the inverse susceptibility is approached also for Co-rich compound in the high temperature limit. The slopes are identical for all samples with $x \geqslant 0.8$, corresponding to $\mu_{\text{eff}} = 3.8\ \mu_B$ ($S = 1.5$). The Weiss constant (or so-called paramagnetic temperature Θ_p) is shifted from the positive $\Theta_p = 250$ K for the FM sample $x = 0.5$ to zero for $x = 0.8$ and, finally, to negative $\Theta_p = -250$ K for $x = 1$. This observation clearly indicates that AFM interactions dominate in $LaCoO_3$ at high temperatures and cobalt ions are either in a mixture of IS and HS Co^{3+} states or charge disproportionated (Co^{2+}/Co^{4+}). The pronounced magnetic anomaly, seen in figure 6 around 550 K for Co-rich samples, is associated with an insulator–metal (I–M) transition and will be discussed later.

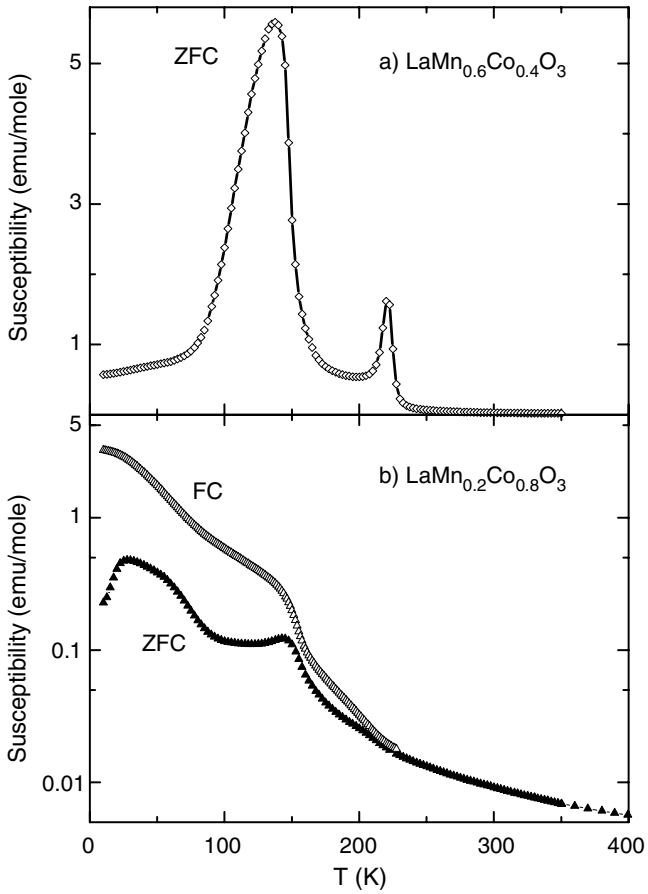

Figure 4. The temperature dependence of the molar susceptibility for ferromagnetic $LaMn_{0.6}Co_{0.4}O_3$ (upper panel) and $LaMn_{0.8}Co_{0.2}O_3$ (lower panel; note the logarithmic scale) measured in a field of 100 Oe. Note the pronounced two-step transition for $x = 0.4$ and the huge difference between the field-cooled and zero-field-cooled curves for $x = 0.8$ below 220 K.

At lower temperatures, the inverse susceptibility for $x = 0.8$–0.95 shows a curvature that is indicative of a tendency to form FM clusters also in these Co-rich samples. A clear anomaly is seen at 150 K and closer inspection may reveal also a kink at about 220 K. The low temperature magnetic behaviour of $LaCoO_3$ deserves special note. The linear part of the inverse susceptibility curve for 150–350 K suggests AFM interactions between Co^{3+} ions with $\Theta_p = -250$ K and the slope corresponds to $\mu_{eff} \sim 3.2\ \mu_B$ ($S \sim 1.2$), just between the theoretical spin-only values for the IS state ($\mu_{eff} \sim 2.83\ \mu_B$) and the average for the LS/HS (1:1) mixture ($\mu_{eff} \sim 3.46\ \mu_B$). In agreement with previous reports on the gradual transition to the Co^{3+} HS or IS species towards the LS ground state (see e.g. [24, 25]), the inverse susceptibility starts to increase below 100 K but sharply turns down below 50 K. This low temperature tail can be ascribed to a paramagnetic impurity, containing possibly Co^{2+} in an amount of about 1%. These states may originate in the surface layers of the perovskite grains as discussed in detail recently [26]. After subtracting the impurity Curie term and temperature-independent van Vleck paramagnetism of Co^{3+} LS ions (expected value $\chi_{vV} = 2 \times 10^{-4}$ emu mol^{-1}) [27], the corrected inverse susceptibility curve diverges at the

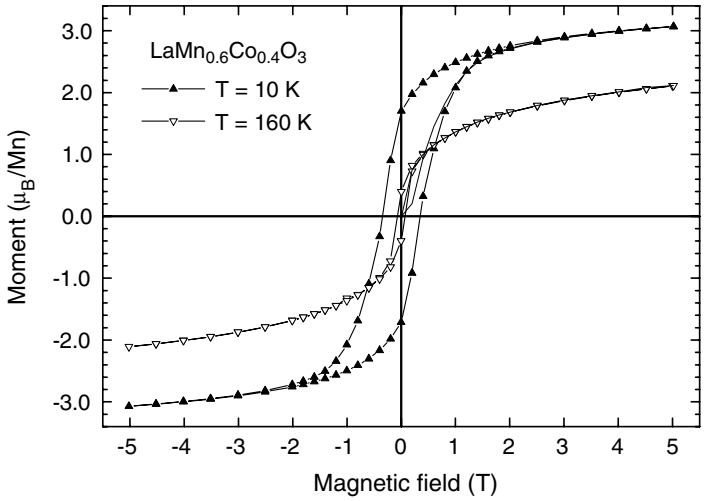

Figure 5. Magnetic hysteresis loops for $LaMn_{0.6}Co_{0.4}O_3$ at $T = 10$ and 160 K.

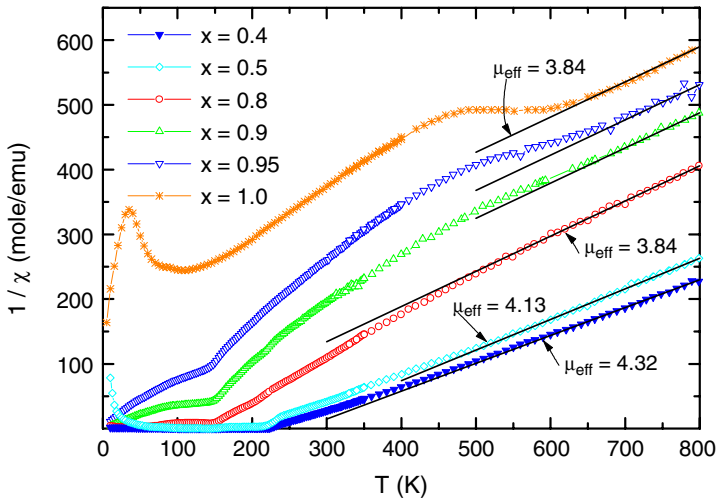

Figure 6. The temperature dependence of the magnetic susceptibility for selected samples from the $LaMn_{1-x}Co_xO_3$ series. The chemical composition is labelled on the graph. The black lines are the high temperature fits.

lowest temperatures, which confirms the orbital and spin singlet state of Co^{3+} in $LaCoO_3$ ($S = 0$).

The electric transport properties of all series $LaMn_{1-x}Co_xO_3$ ($0 \leqslant x \leqslant 1$) are summarized in figures 7 and 8. Whatever the composition, the electrical resistivity curves $\rho(T)$ in figure 7 exhibit an activated type of conductivity up to 900 K. Starting from $LaMnO_3$ the low temperature resistivity (below room temperature) is quickly reduced by Co doping, while beyond $x = 0.2$ this trend is reversed and the resistivity starts to increase and reaches a maximum for the Co content of $x = 0.4$–0.5. For samples with $x \geqslant 0.6$ with rhombohedral symmetry, the resistivity decreases sharply with Co content though the ground state remains insulating. As to the high temperature data, an anomaly is observed in $LaMnO_3$ at the

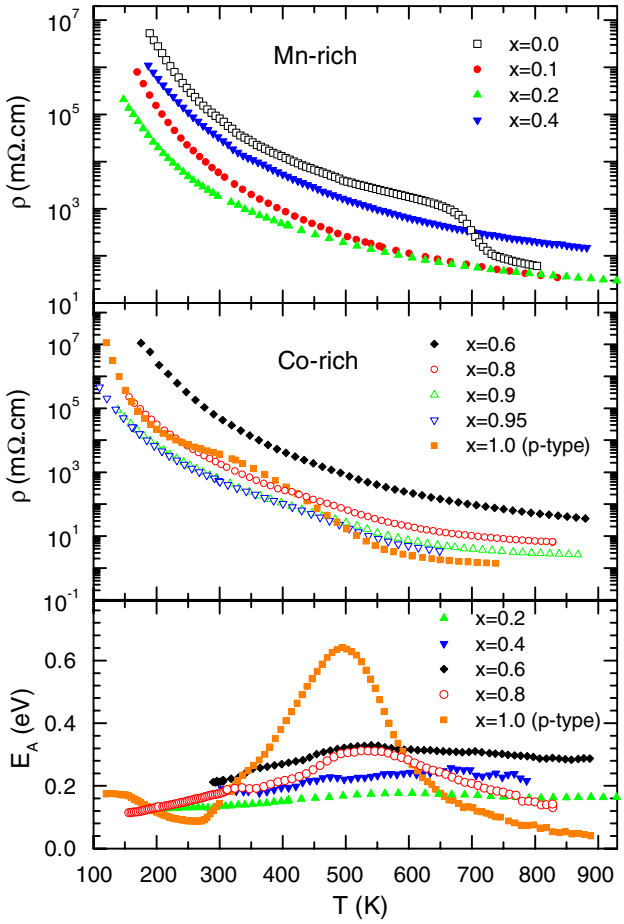

Figure 7. The temperature dependence of the electrical resistivity for $LaMn_{1-x}Co_xO_3$ samples: Mn-rich orthorhombic series with $0.0 \leqslant x \leqslant 0.4$ (upper panel), Co-rich rhombohedral series with $0.6 \leqslant x \leqslant 1.0$ (middle panel). For selected compositions, the temperature dependence of the local activation energy E_A observed as a slope of $\ln(\rho) = f(T^{-1})$ dependence ($E_A = d(\ln(\rho))/d(T^{-1})$) is depicted (lower panel).

cooperative Jahn–Teller transition point $T_{JT} = 700$ K [28] where the resistivity drops by one or two orders of magnitude. In contrast, the $x = 0.1$ sample does not show a similar sharp anomaly, which suggests that the Jahn–Teller transition occurs gradually in this Mn^{3+}-rich compound. On the opposite Co-rich side, one may notice a resistivity drop that occurs at 550 K for samples with $x = 0.9$ and 0.95, in coincidence with the magnetic susceptibility anomaly—see figure 6. A more complex behaviour is observed for $LaCoO_3$. The extrapolation of the low temperature part of the $\rho(T)$ dependence to high temperatures suggests that the resistivity would have saturated at a high value of about 1 Ω cm. This trend is changed just above the room temperature with a marked resistivity decrease that culminates at 500–550 K, as seen in the lower panel of figure 7 in the peak of apparent activation energy $E_A = \partial \ln \rho / \partial T^{-1}$. Finally, a highly conducting state is reached in $LaCoO_3$ as evidenced by the resistivity value of about 1 mΩ cm at the highest temperatures.

The thermoelectric power data in figure 8 show that the thermopower coefficient for pure $LaMnO_3$ at room temperature is high and positive, indicating a small amount of conducting

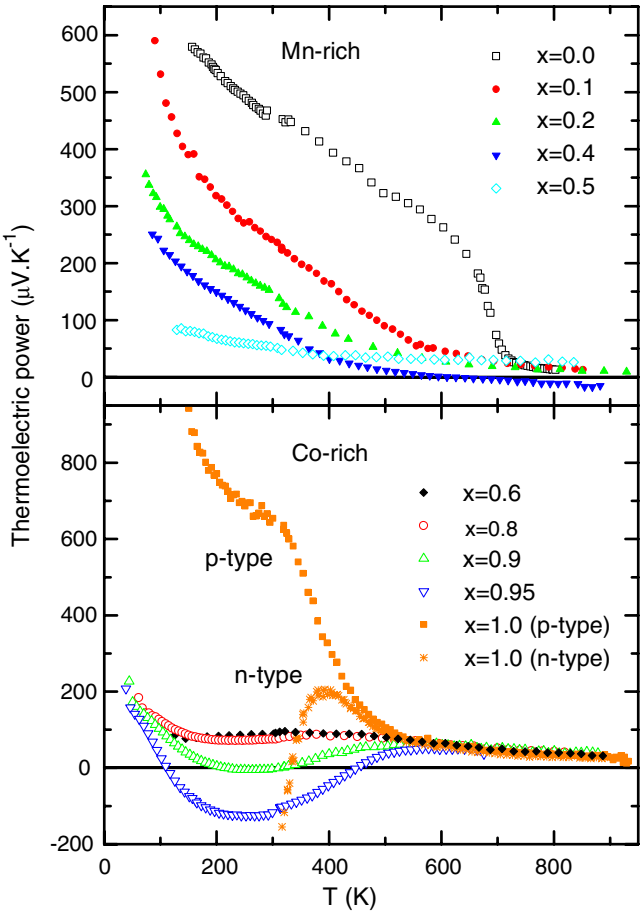

Figure 8. The temperature dependence of the thermoelectric power for the $LaMn_{1-x}Co_xO_3$ series; the chemical composition is labelled on the graph. For the sake of clarity the Mn-rich series ($0.0 \leqslant x \leqslant 0.5$) is shown in the upper panel, the Co-rich series ($0.6 \leqslant x \leqslant 1.0$) in the lower one.

hole-like carriers. A sudden decrease at 700 K is evidently associated with the first-order Jahn–Teller transition. Upon cobalt doping, the thermopower steadily decreases with increasing Co concentration while its temperature dependence preserves an activated character.

The character of the charge carriers may also be deduced from the high temperature part of the thermopower displayed in the upper panel of figure 9, which has similar slopes for the samples with $x = 0.2$–0.4. On the other hand, the high temperature thermopower of the $x = 0.5$ sample is very flat and its positive value at the highest temperatures clearly deviates from the general trend of the former $x = 0.1$–0.4 orthorhombic samples. One may link the temperature-independent thermopower of $x = 0.5$ with hopping of charge carriers where their constant number and degeneracy, as reflected by a temperature-independent thermopower in a wide temperature range, is directly linked with the highest chemical and structural (frontier between the orthorhombic ($x \leqslant 0.5$) and rhombohedral ($x > 0.6$) phases) disorder—see the upper panel of figure 8.

Pure $LaCoO_3$ is characterized by a large thermopower at room temperature, which, depending on the dominating carriers, can be either positive or negative. As regards the p-type sample, the thermopower value $S_{300\ K} = 600\ \mu V\ K^{-1}$ and high and saturating resistivity

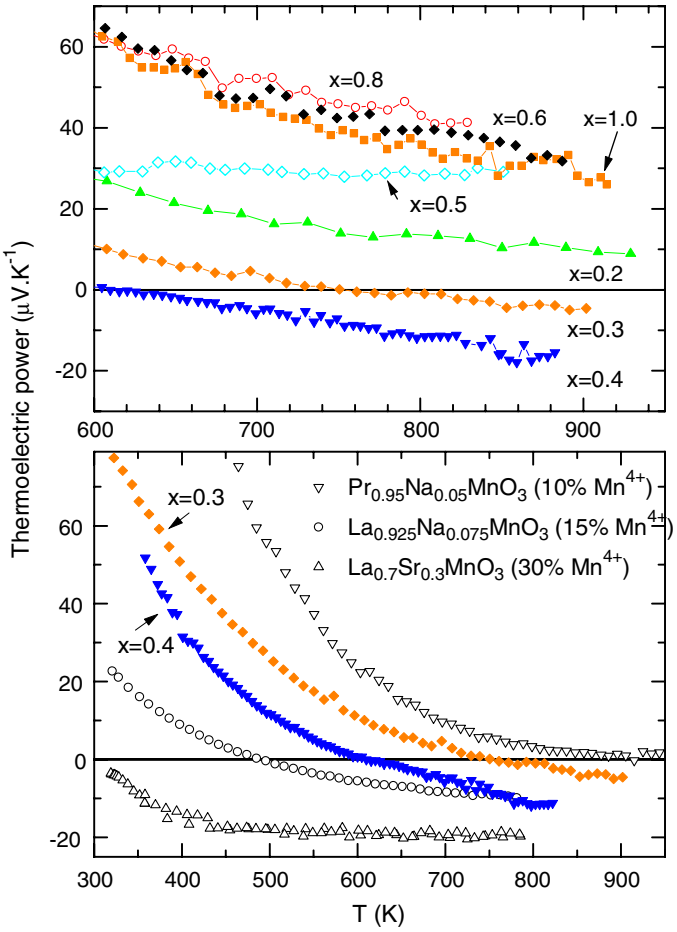

Figure 9. Upper panel: the high temperature (above 600 K) evolution of the thermoelectric power for selected samples of the $LaMn_{1-x}Co_xO_3$ series; the chemical composition is labelled on the graph. Lower panel: the temperature evolution (above 300 K) of the thermoelectric power for $x = 0.3$ and 0.4 samples compared with A-site-substituted manganites.

($\rho_{300\ \mathrm{K}} = 4\ \Omega$ cm), together with extremely low activation energy below room temperature $E_A = 0.09$ eV, point to the hopping mechanism of charge carrier transport involving a small number ($n \sim 10^{19}$ cm^{-3}) of hole-like charge carriers. Above 300 K, the thermopower of p-type $LaCoO_3$ starts to decrease continuously and this broad transition seems to be accomplished at 500–600 K, concurrently with the electrical resistivity and magnetic susceptibility transitions. A specific feature of the n-type $LaCoO_3$ is the change of the n-type to p-type conductivity above 300 K and subsequent downturn of the thermopower above the peak at 400 K to the same high temperature behaviour as found for the p-type case (see figure 9). A similar sign reversal is observed for the slightly Mn-doped compound with $x = 0.95$, as shown in figure 8. For the $x = 0.95$ sample, below the region of negative thermopower between 100 and 400 K, a steep upturn to positive values below is observed. At high temperatures, all Co-rich samples with $x \geqslant 0.6$ including both the p-type and n-type $LaCoO_3$ exhibit the same temperature dependence of the thermopower, decreasing from ~60 μV K^{-1} at 600 K to ~30 μV K^{-1} at 900 K, as demonstrated in figure 9.

4. Discussion

Complexity of the $LaMn_{1-x}Co_xO_3$ properties is associated with the presence of two transition metal ions and variability of their 3d electron configurations. On the basis of the x-ray absorption spectra, Park and Toulemonde *et al* concluded that cobalt in small substitutions enters the perovskite manganates as divalent [15, 29]. The idea of such rigid valency was, however, questioned by Van Elp [30]. According to his analysis, cobalt ions in $LaMn_{1-x}Co_xO_3$ possess a mixed Co^{2+}/Co^{3+} valency with a considerable admixture of the positive charge transferred from the trivalent cobalt to the oxygen ligand, providing the configuration d^7L. Relevant information about the Co and Mn valences can be deduced also from the present measurements of the electric transport and magnetic susceptibility. The transport data coherently show that the absolute values of the both the electrical resistivity and the thermopower at low temperatures decrease sharply upon doping at both ends of the $LaMn_{1-x}Co_xO_3$ series. Taking into account the increased disorder which is inevitably linked with the chemical doping, the increased 'metallicity' of lightly doped $LaMnO_3$ (Co) and $LaCoO_3$ (Mn) should be primarily associated with increasing charge carrier concentration. Consequently, these dopants are stabilized as Co^{2+} in $LaMnO_3$ and Mn^{4+} in $LaCoO_3$. When the respective dopings exceed about 20% ($0.2 < x < 0.9$), the resistivity starts to increase again, probably due to increasing chemical disorder. However, the determination of the valence state of both Co and Mn ions is not so straightforward as for small concentrations. Nevertheless, the valence distribution can be deduced using indirect arguments. In particular, assuming similar hopping mechanisms of charge carrier transport in $LaMn_{1-x}Co_xO_3$ and the A-site-substituted manganites, the thermopower data can serve as important guidance for the estimation of Mn valency for $x > 0.2$. Consequently, comparing the upper and lower panel of figure 9, we infer that the $x = 0.3$ and 0.4 samples exhibit a high temperature course of the thermopower very reminiscent of results observed for manganates $(La, Pr)_{1-y}Na_yMnO_3$ for $y = 0.05$ (10% Mn^{4+}) and $y = 0.075$ (15% Mn^{4+}). Considering thus 12% and 15% Mn^{4+} on manganese sites in the ground state of the present samples with $x = 0.3$ and 0.4, one finds a complex valence distribution, $LaMn^{3+}_{0.62}Mn^{4+}_{0.08}Co^{2+}_{0.08}Co^{3+}_{0.22}O_3$ and $LaMn^{3+}_{0.51}Mn^{4+}_{0.09}Co^{2+}_{0.09}Co^{3+}_{0.31}O_3$, respectively. Supposing high spin Co^{2+}/Co^{3+} states, this distribution gives an average spin value $\langle S\rangle = 1.9$ for the $x = 0.4$ sample, which is in perfect agreement with the high temperature effective moment observed in the susceptibility measurements. We conclude that cobalt, entering $LaMnO_3$ at small rates as Co^{2+}, gradually changes its valence and occurs in the prevailing Co^{3+} state ($\sim$75%) for $x = 0.4$.

An open problem is represented by the qualitative change of thermopower at composition $x = 0.5$. We speculate that mobile carriers belonging to the Mn subsystem localize faster than carriers 'tied' to the Co subsystem as a consequence of local Jahn–Teller distortions around the Mn^{3+} species. The transport within the Co subsystem remains, however, strongly perturbed due to chemical disorder. This leads simultaneously to a high hopping energy $E_H \sim 0.32$ eV as shown in figure 8 and temperature-independent thermoelectric power determined solely by the configurational entropy of hopping carriers [31].

An interesting property of the samples studied, with $x = 0.4$ and 0.5, is the two-step transition to the bulk FM state involving critical temperatures $T_{C1} = 220$ K and $T_{C2} = 150$ K. These two temperatures cannot be attributed solely to a coexistence of the Mn/Co ordered and disordered regions, as suggested previously (see e.g. [17]). First, the neutron diffraction on $x = 0.4$ does not show any signature of the long range Mn/Co cationic order and, secondly, the same two-step FM transition with $T_{C1} = 230$ K and $T_{C2} = 160$ K is observed in pure cobaltite $La_{0.8}Sr_{0.2}CoO_3$, as well. In this latter case, the high resolution diffraction experiments of Caciuffo *et al* [32] provide direct proof of FM clusters of mesoscopic size being present in

Table 3. The thermoelectric power S, electrical resistivity ρ and activation energy E_A at 300 and 800 K for $LaMn_{1-x}Co_xO_3$ solid solutions.

	300 K			800 K		
x	S (μV K^{-1})	ρ (Ω cm)	E_A (meV)	S (μV K^{-1})	ρ (mΩ cm)	E_A (meV)
0	460	80	185	13	60	
0.1	230	5	185	17	40	240
0.2	150	2	135	13	40	160
0.3	120	8	155	0	90	195
0.4	100	30	190	−11	200	230
0.5	55	70	220	29	100	300
0.6	90	65	210	40	50	290
0.8	70	2	175	40	7	170
0.9	0	0.6	150	40	3	120
0.95	−120	0.5	140	35	2	110
1	−200; 600[a]	4	140	35	1	100

[a] n-type; p-type.

the magnetically disordered matrix. The higher critical temperature is ascribed to the local T_C of the slowly fluctuating clusters, while the lower critical temperature is simply interpreted as the global T_C. 'Glassy' ferromagnetism in $La_{1-x}Sr_xCoO_3$ is evidenced also in a recent paper of Wu and Leighton [33]. The two-step behaviour can thus be related to an intrinsic chemical inhomogeneity of $La_{1-x}Sr_xCoO_3$ or $LaMn_{1-x}Co_xO_3$ solid solutions, which gives rise to a broad distribution of magnetic interactions (realization of a Griffiths phase). The spatial extent of the short range fluctuations of the chemical composition can be eventually minimized in samples quenched from high temperatures and enhanced for samples sintered at low temperatures (see [18]).

With a further increase of x, the Co subsystem in $LaMn_{1-x}Co_xO_3$ is less perturbed by the Mn neighbours and, simultaneously, the mixed Mn^{3+}/Mn^{4+} valency is continuously transformed to the dominating Mn^{4+} one. In the insulating low temperature state, the charge excess induced by Mn^{4+} valency is compensated by Co^{2+} ions providing electrons, which can—though it is very hard—hop within the Co^{3+} matrix. This is probably at the root of the gradual depression of thermopower with x in the 100–400 K region towards negative values—see figure 8.

As to valence states and properties of charge carriers in the high temperature region, reference can be made to table 3 where the values of the thermopower coefficient, electrical resistivity and its activation energy at 300 and 800 K are summarized. The data at 800 K reflect a hopping regime where effects of grain boundaries and defects become marginal with respect to the overwhelming role of phonon scattering and substitutional disorder. Two compositional regions are distinguishable. As already pointed out, the transport in the first region $0 \leqslant x \leqslant 0.4$ takes place via hopping of holes over the Mn sites, while the Co subsystem remains insulating. The thermopower at 800 K shows a weakly composition-dependent value $S_{800} \sim 13$ μV K^{-1} up to $x = 0.2$; then a rapid decrease is observed towards $S_{800} = -11$ μV K^{-1} for $x = 0.4$. The electrical conduction in $LaMnO_3$, above the Jahn–Teller transition temperature, should be attributed to carriers that arise due to dynamic disproportionation, $Mn^{3+} + Mn^{3+} \rightarrow Mn^{2+} + Mn^{4+}$ [23]. The Co substitution necessarily modifies the carrier concentration but, taking into account the dominance of the dynamic disproportionation effect, it plays only a secondary role in the high temperature transport.

In the second compositional region, $0.6 \leqslant x \leqslant 1.0$, the high temperature resistivity decreases drastically with x and achieves the lowest values for the $LaCoO_3$ ceramics,

$\rho_{800} \sim 1$ mΩ cm. On the other hand, the transport in Mn-doped samples is characterized by quickly increasing activation energy from $E_{A,800} = 0.10$ eV for $x = 1$ to 0.17 eV for $x = 0.8$. Importantly, the thermopower coefficient shows a similar value for all the rhombohedral samples, $S_{800} \sim 35$–40 μV K^{-1}. These findings imply that for the $x > 0.6$ samples the high temperature conduction takes place via hopping within the cobalt subsystem, the carrier concentration being high and not critically influenced by Mn content. We thus conclude that manganese dopants are active in the high temperature electrical transport as significant scattering.

5. Conclusions

The solid solutions $LaMn_{1-x}Co_xO_3$ form perovskite structures with either orthorhombic (Mn-rich side) or rhombohedral (Co-rich side) symmetry. The orthorhombic to rhombohedral boundary is located at composition $x \approx 0.6$. The analysis of transport properties in the orthorhombic region indicates that cobalt enters $LaMnO_3$ as Co^{2+} for low x and induces fluctuating Mn^{3+}/Mn^{4+} valence states. However, the carrier concentration is not simply proportional to x, but saturates for the higher x. Thus for $x \sim 0.4$ the majority of transition metal ions were assigned, on the basis of electric and magnetic data, to the majority Mn^{3+} and Co^{3+} states, where the Co^{2+} or Mn^{4+} states represent a minor faction.

A more detailed investigation using neutron diffraction and magnetization measurements was undertaken on a sample with $x = 0.4$ which exhibits a two-step transition to the bulk FM state. It is argued that this anomalous behaviour should be related to intrinsic chemical fluctuations, common for complex oxides, and need not be associated with the coexistence of the Mn/Co ordered and disordered regions.

The investigation of the rhombohedral region of the $LaMn_{1-x}Co_xO_3$ series shows that manganese enters $LaCoO_3$ preferentially as Mn^{4+} and induces electron-like carriers in the Co–O subarray. The low temperature electrical transport is then influenced by hopping electrons within the Co^{3+} matrix. At elevated temperatures, however, a small positive and weakly temperature-dependent thermopower together with a low electrical resistivity observed in $LaMn_{1-x}Co_xO_3$ ($0.6 \leqslant x \leqslant 1$) indicate the presence of new kinds of thermally activated hole-like carriers. This situation is most clearly demonstrated in the originally insulating $LaCoO_3$ when, above 500–600 K, the carrier concentration seems to be saturated; the resistivity drops sharply and achieves a quasimetallic value of $\sim$1 mΩ cm. The effective moments for $x = 0.8$–1, reflected in the Curie–Weiss susceptibility law, approach above 600 K a constant value corresponding to spin number $S \sim 1.5$. Taking these data into account, the high temperature behaviour of the Co-rich $LaMn_{1-x}Co_xO_3$ perovskites can be explained supposing a dynamic disproportionation of formally IS Co^{3+} ions into IS Co^{4+} + HS Co^{2+} pairs (similar to the disproportionation of Mn^{3+} into $Mn^{4+} + Mn^{2+}$ suggested for $LaMnO_3$ above 700 K). This effect promotes extra electrons into cobalt e_g states, resulting in an antibonding σ^* band that is more than half-filled. The e_g electrons remain, however, strongly correlated, which critically limits their degeneracy and favours 'hopping' in contrast to the 'band' character of the transport mechanism.

Acknowledgments

The work was supported by the Grant Agency of the Czech Republic, grant No. 203/03/0924, and by the programme KONTAKT ME 572 of the Ministry of Education, Youth and Sports of the Czech Republic. One of us (CA) is grateful for financial support provided through the

European Community's Human Potential Programme under contract HPRN-CT-2002-00293, SCOOTMO.

References

[1] Tokura Y 2000 *Colossal Magnetoresistive Oxides* (New York: Gordon and Breach)
[2] Rao C N R and Raveau B 1998 *Colossal Magnetoresistance, Charge Ordering and Related Properties of Manganese Oxides* (Singapore: World Scientific)
[3] Rodríguez-Carvajal J, Hennion M, Moussa F, Moudden A H, Pinsard L and Revcolevschi A 1998 *Phys. Rev.* B **57** R3189
[4] Töpfer J and Goodenough J B 1997 *J. Solid State Chem.* **130** 117
[5] Ritter C, Ibarra M R, De Teresa J M, Algarabel P A, Marquina C, Blasco J, García J, Oseroff S and Cheong S-W 1997 *Phys. Rev.* B **56** 8902
[6] Senarís-Rodríguez M A and Goodenough J B 1995 *J. Solid State Chem.* **116** 224
[7] Korotin M A, Ezhov S Yu, Solovyev I V and Anisimov V I 1996 *Phys. Rev.* B **54** 5309
[8] Saitoh T, Mizokawa T, Fujimori A, Abbate M, Takeda Y and Takano M 1997 *Phys. Rev.* B **55** 4257
[9] Yamaguchi S, Okimoto Y and Tokura Y 1997 *Phys. Rev.* B **55** 8666
[10] Asai K, Yoneda A, Yokokura O, Tranquada J M, Shirane G and Kohn K 1998 *J. Phys. Soc. Japan* **67** 290
[11] Kobayashi Y, Fujiwara N, Murata S, Asai K and Yasuska H 2000 *Phys. Rev.* B **62** 410
[12] Radaelli P G and Cheong S-W 2002 *Phys. Rev.* B **66** 094408
[13] Goodenough J B, Wold A, Arnott R J and Menyuk N 1961 *Phys. Rev.* **124** 373
[14] Blasse G 1965 *J. Phys. Chem. Solids* **26** 1969
[15] Park J-H, Cheong S-W and Chen C T 1997 *Phys. Rev.* B **55** 11072
[16] Troyanchuk O, Lobanovsky L S, Khalyavin D D, Pastushonok S N and Szymczak H 2000 *J. Magn. Magn. Mater.* **210** 63
[17] Dass R I and Goodenough J B 2003 *Phys. Rev.* B **67** 014401
[18] Joy P A, Khollam Y B, Patole S N and Date S K 2000 *Mater. Lett.* **46** 261
[19] Joy P A, Khollam Y B and Date S K 2000 *Phys. Rev.* B **62** 8608
[20] Bull C L, Gleeson D and Knight K S 2003 *J. Phys.: Condens. Matter* **15** 4927
[21] Voronin V I, Karkin A E, Petrov A N, Pirogov A N, Cherepanov V A, Teplych A E and Filonova E A 1997 *Physica* B **234–236** 710
[22] Vogt T, Hriljac J A, Hyatt N C and Woodward P 2003 *Phys. Rev.* B **67** 140401
[23] Zhou J-S, Yin H Q and Goodenough J B 2001 *Phys. Rev.* B **63** 184423
[24] Zobel C, Kriener M, Bruns D, Baier J, Gruninger M, Lorenz T, Reutler P and Revcolevschi A 2002 *Phys. Rev.* B **66** 020402
[25] Yan J-Q, Zhou J-S and Goodenough J B 2004 *Phys. Rev.* B **69** 134409
[26] Yan J-Q, Zhou J-S and Goodenough J B 2004 *Phys. Rev.* B **70** 01440
[27] Kamimura H 1966 *J. Phys. Soc. Japan* **3** 48
[28] Zhou J-S and Goodenough J B 1999 *Phys. Rev.* B **60** R15002
[29] Toulemonde O, Studer F and Raveau B 2001 *Solid State Commun.* **118** 107
[30] Van Elp J 1999 *Phys. Rev.* B **60** 7649
[31] see e.g. Chaikin P M 1990 An introduction to thermopower *Organic Superconductivity* ed V Z Kresin and W A Little (New York: Plenum)
[32] Caciuffo R, Rinaldi D, Barucca G, Mira J, Rivas J, Senarís-Rodríguez M A, Radaelli P G, Fiorani D and Goodenough J B 1999 *Phys. Rev.* B **59** 1068
[33] Wu J and Leighton C 2003 *Phys. Rev.* B **67** 174408